C. R. Mecanique 344 (2016) 759–768

Contents lists available at ScienceDirect

Comptes Rendus Mecanique

www.sciencedirect.com

The Proper Generalized Decomposition as a space–time integrator for elastoplastic problems

Jean-Michel Bergheau [a], Sylvain Zuchiatti [a], Jean-Christophe Roux [a,*], Éric Feulvarch [a], Samuel Tissot [b], Gilles Perrin [c]

[a] Université de Lyon, ENISE, LTDS, UMR 5513 CNRS, 58, rue Jean-Parot, 42023 Saint-Étienne cedex 2, France
[b] AREVA NP, 10–12, rue Juliette-Récamier, 69456 Lyon cedex 06, France
[c] AREVA NP, Tour Areva, 1, place Jean-Millier, 92084 Paris La Défense cedex, France

ARTICLE INFO

Article history:
Received 11 February 2016
Accepted 28 June 2016
Available online 6 September 2016

Keywords:
Proper Generalized Decomposition
Space–time finite elements
Elastoplasticity

ABSTRACT

This paper details the development of the Proper Generalized Decomposition as a space–time integrator of elastoplastic problems and shows its ability to determine the elastoplastic states resulting from cyclic loadings. The first part of this paper recalls the step-by-step resolution in time of an elastoplastic problem. The implementation of the Proper Generalized Decomposition is then developed in a second part. In the last third part, applications and numerical simulations are presented to show the relevance of the method.

© 2016 Académie des sciences. Published by Elsevier Masson SAS. This is an open access article under the CC BY-NC-ND license (http://creativecommons.org/licenses/by-nc-nd/4.0/).

1. Introduction

The prediction of the fatigue life span of mechanical components requires a good knowledge of the stabilized cyclic mechanical states. Thermomechanical loads applied periodically to a structure can indeed lead to various limit states.

- The elastic shakedown: the cyclic behavior at any point of the structure is then elastic. A plastic deformation can develop during the first cycles but ends up being stabilized. The lifespan analyses are then based on high-cycle fatigue criteria.
- The plastic shakedown: the cyclic behavior in each point stabilizes in that case on an elastoplastic cycle, which is repeated during the following cycles. The lifespan analyses then require low-cycle (oligocyclic) fatigue criteria.
- The cyclic ratcheting behavior: it then appears a progressive deformation that increments cycle after cycle. This phenomenon is related to the behavior of material combined with certain types of loading and can lead to the ruin of the structure.

The search for these limit states by a classical step-by-step method can lead to extremely long computation times. In practice, such a method can become unusable when the number of cycles is very high.

* Corresponding author.
E-mail addresses: jean-michel.bergheau@enise.fr (J.-M. Bergheau), sylvain.zuchiatti@enise.fr (S. Zuchiatti), jean-christophe.roux@enise.fr (J.-C. Roux), eric.feulvarch@enise.fr (É. Feulvarch), samuel.tissot@areva.com (S. Tissot), gilles.perrin@areva.com (G. Perrin).

http://dx.doi.org/10.1016/j.crme.2016.06.002
1631-0721/© 2016 Académie des sciences. Published by Elsevier Masson SAS. This is an open access article under the CC BY-NC-ND license (http://creativecommons.org/licenses/by-nc-nd/4.0/).

To predict the limit states, several authors then proposed simplified methods that are based on estimates of the parameters of the stabilized state [1–3]. Peigney and Stolz [4] proposed an approach using optimal control and Maitournam et al. [5] developed a direct research method of the limit states by decomposing in Fourier series the equations and the variables of the problem. Other common practices in industry consist in searching the stabilized states starting from a step-by-step calculation, but by using a behavior model identified on the material's cyclic curve, in such a way as to obtain the stabilized states in only some cycles. Other authors like Lesne and Savalle [6], Chaboche and Cailletaud [7] have sought to reduce the simulation times by reducing the number of simulated cycles by means of a method of jumps of cycles.

Finally, alternative methods to the step-by-step calculations of the elastoplastic transients have also been developed. These methods are generally based on the convergence of an iterative process between a global resolution of the equilibrium equations on the whole analysis time interval to obtain a solution that is statically and kinematically admissible, and a local resolution of the constitutive equations for the calculation of the plastic correction of the stresses. The Large Time Increment (LATIN) method is, in the authors' knowledge, the first method suggested in this domain [8,9]; more recently Comte et al. [10] proposed an alternative by projecting the global equations on a basis of wavelets.

The method that we propose in this article falls within this last category. It aims at reducing the computation times by using the "Proper Generalized Decomposition" (PGD) as a space–time integrator of the elastoplastic problem to determine the elastoplastic (or viscoplastic) states resulting from cyclic thermomechanical loads, but more generally from any type of loading.

The PGD is a method of model reduction whose principle consists in seeking a global solution to a problem involving numerous variables (space variables, time, various parameters) by separating these variables [11–13]. One thus seeks the solution in the form of a sum of modes, each mode being calculated as a product of functions of each of the considered variables. The PGD is an *a priori* method and does not require the calculation of a reference basis, contrary to the "Proper Orthogonal Decomposition" (POD) method introduced by Lumley [14].

Although the convergence of the method is not yet demonstrated in a general way, recent works showed a satisfactory numerical behavior in solid mechanics [15], and more particularly in the treatment of viscoelasticity [16,17].

2. In-time step-by-step resolution of elastoplastic problems

2.1. Weak formulation

The problem we propose to solve is governed at any instant $t \in T = [0, \tau]$ by the equilibrium equations of a continuous medium supplied with the usual boundary conditions:

$$\begin{cases} \mathbf{div}(\boldsymbol{\sigma}) + \boldsymbol{f_v} = \mathbf{0} & \text{in } \Omega \quad \text{(a)} \\ \boldsymbol{\sigma} \cdot \mathbf{n} = \boldsymbol{T}^p & \text{on } \Gamma_T \quad \text{(b)} \\ \boldsymbol{u} = \mathbf{0} & \text{on } \Gamma_u \quad \text{(b)} \end{cases} \tag{1}$$

In these equations, $T = [0, \tau]$ is the time interval of analysis; Ω is the spatial domain of the study, of boundary $\partial\Omega = \Gamma_T \cup \Gamma_u$; $\boldsymbol{\sigma}(\boldsymbol{x}, t)$ is the Cauchy stress tensor; $\boldsymbol{u}(\boldsymbol{x}, t)$ is the displacement vector; $\boldsymbol{f_v}(\boldsymbol{x}, t)$ represents volume forces and $\boldsymbol{T}^p(\boldsymbol{x}, t)$, surface forces; $\mathbf{n}$ is the unit outward normal vector to the boundary $\partial\Omega$. Note that the loads can be time dependent.

Here we place ourselves within the framework of the infinitesimal strain theory. At any instant and at any point, $\boldsymbol{\sigma}(\boldsymbol{x}, t)$ is connected to the history of strain $\boldsymbol{\varepsilon}(\boldsymbol{x}, t)$ at the same point by the constitutive equations of elastoplasticity (or elastoviscoplasticity). Any behavioral model can be used at this stage; more generally, the method presented below can be applied such as it is to other types of constitutive equations.

The classical resolution of elastoplastic problems by a step-by-step finite-element approach is based on the following weak formulation (itself very classical), which consists in searching, at each time t, the displacement field $\boldsymbol{u}(\boldsymbol{x}, t)$ verifying:

$$\forall \boldsymbol{v}^*(\boldsymbol{x}), \quad \int_\Omega \boldsymbol{v}^*(\boldsymbol{x}) \cdot \boldsymbol{f_v}(\boldsymbol{x}, t)\, \mathrm{d}\omega + \int_{\Gamma_T} \boldsymbol{v}^*(\boldsymbol{x}) \cdot \boldsymbol{T}^p(\boldsymbol{x}, t)\, \mathrm{ds} - \int_\Omega \boldsymbol{\varepsilon}\left(\boldsymbol{v}^*(\boldsymbol{x})\right) : \boldsymbol{\sigma}(\boldsymbol{x}, t)\, \mathrm{d}\omega = 0 \tag{2}$$

where $\boldsymbol{v}^*(\boldsymbol{x})$ are test functions and $\boldsymbol{\varepsilon}(\boldsymbol{v}^*) = \frac{1}{2}\left(\mathbf{grad}\, \boldsymbol{v}^* + \mathbf{grad}^{\mathrm{t}}\, \boldsymbol{v}^*\right)$.

Let us note that the mechanical state depends on time t only through the loading. In fact, the time t is only useful to describe the loading history, the inertial forces being neglected.

2.2. Finite-element problem

On the basis of the weak formulation (2), the application of a finite-element approximation (in space) to the problem (1) leads to search at each time the displacement field $\boldsymbol{u}(\boldsymbol{x}, t)$ in the following form, inside each element [18,19]:

$$\boldsymbol{u}(\boldsymbol{x}, t) = \sum_{i=1}^{n^e} N_i^e(\boldsymbol{x})\, \boldsymbol{U_i}^e(t) = \boldsymbol{N}^e(\boldsymbol{x}) \cdot \boldsymbol{U}^e(t) \tag{3}$$

where $\boldsymbol{N}^e(\boldsymbol{x})$ and $\boldsymbol{U}^e(t)$ represent respectively the array of element shape functions and the vector of nodes' displacements for the element e at time t. For clearness reasons, we will omit the reference to the element ^{e} in the sequel and write: $\boldsymbol{u}(\boldsymbol{x},t) = \boldsymbol{N}(\boldsymbol{x})\cdot\boldsymbol{U}(t)$. The test functions will be also written in the form: $\boldsymbol{v}^*(\boldsymbol{x}) = \boldsymbol{N}\cdot\boldsymbol{V}^*$.

The problem (2) can thus be stated in the following form.

Find at each time t the vector of nodal displacements $\boldsymbol{U}(t)$ such that:

$$\forall\, \boldsymbol{V}^*, \quad \boldsymbol{V}^{*\mathrm{t}}\cdot\boldsymbol{R}(t) = 0$$

i.e. such that:

$$\boldsymbol{R}(t) = 0 \tag{4}$$

In equation (4), $\boldsymbol{R}(t)$ represents the vector of instantaneous nodal residuals at time t, which results from the assembly of the elementary residuals $\boldsymbol{R}^{\boldsymbol{e}}(t)$. Its expression immediately comes from Eq. (2) wherein the approximation scheme (3) is injected:

$$\boldsymbol{R}(t) = \int_{\Omega} \boldsymbol{N}(\boldsymbol{x})^{\mathrm{t}}\cdot\boldsymbol{f_v}(\boldsymbol{x},t)\,\mathrm{d}\omega + \int_{\Gamma_T} \boldsymbol{N}(\boldsymbol{x})^{\mathrm{t}}\cdot\boldsymbol{T}^p(\boldsymbol{x},t)\,\mathrm{ds} - \int_{\Omega} \boldsymbol{B}(\boldsymbol{x})^{\mathrm{t}}\cdot\boldsymbol{\sigma}(\boldsymbol{x},t)\,\mathrm{d}\omega \tag{5}$$

where $\boldsymbol{B}(\boldsymbol{x})^{\mathrm{t}}$ represents the matrix which allows to pass from nodal displacements to the components of the strain tensor and where $\boldsymbol{\sigma}(\boldsymbol{x},t) = (\sigma_{11}\,\sigma_{22}\,\sigma_{33}\,\sigma_{12}\,\sigma_{13}\,\sigma_{23})^{\mathrm{t}}$ represents the classical notation of Voigt for the components of the stress tensor.

Note that the vector of instantaneous residuals $\boldsymbol{R}(t)$ depends on time through the loading (which is a data) and the state of stress at any point, which himself depends on the history of deformation and thus on the history of displacement until the time t.

The various integrals appearing in Eq. (5) are computed by Gauss integration. At each Gauss point, the stress state is calculated step by step in time using a suited algorithm (of 'radial return' type), which depends on the constitutive equations considered (see, for example, [20,21]).

The resolution of the problem (4) can be achieved using the Newton–Raphson method (see for example [22]) and gives the displacement vector $\boldsymbol{U}(t)$ at each loading step.

3. Implementation of the Proper Generalized Decomposition

3.1. Principle

The Proper Generalized Decomposition (PGD) consists in seeking the solutions to a problem using the separation of variables. In our case, we apply it to the resolution of elastoplastic problems by looking for solutions by separating the variables of space $\boldsymbol{x}$ and of time t.

The aim is thus to approximate the field of displacement by a sequence of functions $\boldsymbol{u_M}(\boldsymbol{x},t)$ of the following form:

$$\boldsymbol{u_M}(\boldsymbol{x},t) = \sum_{\alpha=1}^{M} \boldsymbol{d_\alpha}(\boldsymbol{x})\, f_\alpha(t) \tag{6}$$

where the functions $\boldsymbol{d_\alpha}(\boldsymbol{x})$ and $f_\alpha(t)$ are now looked for by finite-element approximations in space for $\boldsymbol{d_\alpha}(\boldsymbol{x})$ and in time for $f_\alpha(t)$. Therefore we do not intend any more to solve the problem step by step in time, but globally on the whole time interval $T = [0,\tau]$ of the study.

The search for the modes in space and in time is performed iteratively, mode after mode. Thus, having an approximation $\boldsymbol{u}_M(\boldsymbol{x},t)$ until an order M, we look for a couple of functions $(\boldsymbol{d}_{M+1}(\boldsymbol{x}), f_{M+1}(t))$ such that $\boldsymbol{u}_{M+1}(\boldsymbol{x},t) = \boldsymbol{u}_M(\boldsymbol{x},t) + \boldsymbol{d}_{M+1}(\boldsymbol{x})\, f_{M+1}(t)$ constitutes a better approximation of the solution $\boldsymbol{u}(\boldsymbol{x},t)$.

3.2. Weak formulation

To apply the finite element method in space and in time, the weak formulation of the problem is now obtained by multiplying Eq. (1)(a) by weight functions $\boldsymbol{v}^*(\boldsymbol{x},t)$ that are written in the form:

$$\boldsymbol{v}^*(\boldsymbol{x},t) = \boldsymbol{d}^*(\boldsymbol{x})\, f(t) + \boldsymbol{d}(\boldsymbol{x})\, f^*(t) \tag{7}$$

and then by integrating the result on the time interval T and the space domain Ω. Let us note that in Eq. (7), the searched functions of the variables of space and time are noted $\boldsymbol{d}(\boldsymbol{x})$ and $f(t)$ to reduce the writing. Integrating by part on the space domain Ω and taking into account the boundary conditions (1)(b)(1)(c), the variational problem becomes:

Find $\boldsymbol{d}(\boldsymbol{x})$ and $f(t)$ such that:

$$\forall \boldsymbol{v}^*(\boldsymbol{x},t),\quad \int_T \int_\Omega \boldsymbol{v}^*(\boldsymbol{x},t)\cdot\boldsymbol{f}_v(\boldsymbol{x},t)\,\mathrm{d}\omega\,\mathrm{d}t + \int_T \int_{\Gamma_T} \boldsymbol{v}^*(\boldsymbol{x},t)\cdot\boldsymbol{T}^p(\boldsymbol{x},t)\,\mathrm{d}s\,\mathrm{d}t - \int_T \int_\Omega \boldsymbol{\varepsilon}\left(\boldsymbol{v}^*(\boldsymbol{x},t)\right) : \boldsymbol{\sigma}(\boldsymbol{x},t)\,\mathrm{d}\omega\,\mathrm{d}t = 0 \tag{8}$$

As Eq. (8) must be satisfied whatever $\boldsymbol{v}^*$ given by Eq. (7), it must be satisfied whatever $\boldsymbol{d}^*$ and f^* independently:

$$\forall \boldsymbol{d}^*(\boldsymbol{x}),\quad \int_T f(t)\int_\Omega \boldsymbol{d}^*(\boldsymbol{x})\cdot\boldsymbol{f}_v(\boldsymbol{x},t)\,\mathrm{d}\omega\,\mathrm{d}t + \int_T f(t)\int_{\Gamma_T} \boldsymbol{d}^*(\boldsymbol{x})\cdot\boldsymbol{T}^p(\boldsymbol{x},t)\,\mathrm{d}s\,\mathrm{d}t - \int_T f(t)\int_\Omega \boldsymbol{\varepsilon}\left(\boldsymbol{d}^*(\boldsymbol{x})\right) : \boldsymbol{\sigma}(\boldsymbol{x},t)\,\mathrm{d}\omega\,\mathrm{d}t = 0 \tag{9a}$$

$$\forall f^*(t),\quad \int_T f^*(t)\int_\Omega \boldsymbol{d}(\boldsymbol{x})\cdot\boldsymbol{f}_v(\boldsymbol{x},t)\,\mathrm{d}\omega\,\mathrm{d}t + \int_T f^*(t)\int_{\Gamma_T} \boldsymbol{d}(\boldsymbol{x})\cdot\boldsymbol{T}^p(\boldsymbol{x},t)\,\mathrm{d}s\,\mathrm{d}t - \int_T f^*(t)\int_\Omega \boldsymbol{\varepsilon}\left(\boldsymbol{d}(\boldsymbol{x})\right) : \boldsymbol{\sigma}(\boldsymbol{x},t)\,\mathrm{d}\omega\,\mathrm{d}t = 0 \tag{9b}$$

The weak formulation of the problem now consists of two variational equations, one relative to the function of space variables (9a) and the other one to the function of time (9b).

After resolution, we set $\boldsymbol{d}_{M+1}(\boldsymbol{x}) = \boldsymbol{d}(\boldsymbol{x})$ and $f_{M+1}(t) = f(t)$, and we move on to the next mode. The strategy of resolution will be discussed in section 4 for the discrete problem.

3.3. Finite-element formulation

We consider a mesh of the spatial domain Ω. The field $\boldsymbol{d}(\boldsymbol{x})$ is sought in the following form:

$$\boldsymbol{d}(\boldsymbol{x}) = \boldsymbol{N}(\boldsymbol{x})\cdot\boldsymbol{D} \tag{10}$$

where $\boldsymbol{N}(\boldsymbol{x})$ and $\boldsymbol{D}$ represent respectively the array of element shape functions and the vector of nodal values of $\boldsymbol{d}(\boldsymbol{x})$. The field $\boldsymbol{d}^*(\boldsymbol{x})$ is approximate in the same way by $\boldsymbol{d}^*(\boldsymbol{x}) = \boldsymbol{N}(\boldsymbol{x})\cdot\boldsymbol{D}^*$.

The time domain $T = [0,\tau]$ is subdivided in time sub-intervals representing finite elements in time. The ends of the sub-intervals are the temporal nodes to which correspond various times t_i. The temporal nodes are numbered from 1 to N_T per ascending order of the times t_i to which they correspond. We denote F_i the value of the time function at the ith temporal node *i.e.* at time t_i. The approximation of the function $f(t)$ can then be written as:

$$f(t) = \boldsymbol{P}(t)\cdot\boldsymbol{F} \tag{11}$$

where $\boldsymbol{P}(t)$ and $\boldsymbol{F}$ represent respectively the array of shape functions of the temporal elements and the vector of the values of function $f(t)$ at temporal nodes. $f^*(t)$ is approximate in the same manner by $f^*(t) = \boldsymbol{P}(t)\cdot\boldsymbol{F}^*$. Notice that, considering equations (10) and (11), (6) becomes $\boldsymbol{u}_{\boldsymbol{M}}(\boldsymbol{x},t) = \boldsymbol{N}(\boldsymbol{x})\cdot\boldsymbol{U}(t)_M$ with:

$$\boldsymbol{U}(t)_M = \sum_{\alpha=1}^{M} \boldsymbol{D}_\alpha\cdot\boldsymbol{P}(t)^{\mathrm{t}}\cdot\boldsymbol{F}_\alpha \tag{12}$$

where $\boldsymbol{U}(t)_M$ is the vector of displacements of the nodes of the space domain during time obtained with M modes and $\boldsymbol{D}_\alpha$, $\boldsymbol{F}_\alpha$ $(\alpha = 1,\ldots,M)$ are the computed modes in space and in time.

With the schemes of approximation (10) and (11), the variational problem (9) is thus equivalent to find $\boldsymbol{D}$ and $\boldsymbol{F}$ such that:

$$\int_T f(t)\left(\int_\Omega \boldsymbol{N}(\boldsymbol{x})^{\mathrm{t}}\cdot\boldsymbol{f}_v(\boldsymbol{x},t)\,\mathrm{d}\omega + \int_{\Gamma_T} \boldsymbol{N}(\boldsymbol{x})^{\mathrm{t}}\cdot\boldsymbol{T}^p(\boldsymbol{x},t)\,\mathrm{d}s - \int_\Omega \boldsymbol{B}(\boldsymbol{x})^{\mathrm{t}}\cdot\boldsymbol{\sigma}(\boldsymbol{x},t)\,\mathrm{d}\omega\right)\mathrm{d}t = 0$$

$$\int_T \boldsymbol{P}(t)\cdot\boldsymbol{D}\left(\int_\Omega \boldsymbol{N}(\boldsymbol{x})^{\mathrm{t}}\cdot\boldsymbol{f}_v(\boldsymbol{x},t)\,\mathrm{d}\omega + \int_{\Gamma_T} \boldsymbol{N}(\boldsymbol{x})^{\mathrm{t}}\cdot\boldsymbol{T}^p(\boldsymbol{x},t)\,\mathrm{d}s - \int_\Omega \boldsymbol{B}(\boldsymbol{x})^{\mathrm{t}}\cdot\boldsymbol{\sigma}(\boldsymbol{x},t)\,\mathrm{d}\omega\right)\mathrm{d}t = 0$$

that we can rewrite with Eq. (5) under the form:

$$\boldsymbol{\varphi}_{\Omega} = \int_T f(t)\,\boldsymbol{R}(t)\,\mathrm{d}t = 0 \tag{13a}$$

$$\boldsymbol{\psi}_T = \int_T \boldsymbol{P}(t)\cdot\boldsymbol{D}^{\mathrm{t}}\cdot\boldsymbol{R}(t)\,\mathrm{d}t = 0 \tag{13b}$$

Equation (13a) defines the residual in space whose dimension is equal to 3 times the number of nodes of the space domain Ω (in 3D). Equation (13b) defines the residual in time; its dimension is equal to the number of temporal nodes.

Remark 3.1. In elastoplasticity, and more generally in non-linear problems, the integrals in space and time are not easily separable. As proposed in the LATIN method, one could use a Proper Orthogonal Decomposition [23]. But experience shows that this approach can introduce a numerical noise detrimental for the calculation quality [24]. In this work, the stresses $\boldsymbol{\sigma}(\boldsymbol{x},t)$ are calculated in a standard way, step by step in time without decomposition. Therefore, Eqs. (13a) and (13b) are still coupled despite the PGD decomposition of the displacement field.

Let us notice that $\boldsymbol{\varphi}_{\Omega}$ and $\boldsymbol{\psi}_T$ depend nonlinearly on $\boldsymbol{D}$ and on $\boldsymbol{F}$ through the vector of the instantaneous residuals $\boldsymbol{R}(t)$ defined by Eq. (5), which depends at each time on

$$\boldsymbol{U}(t)_{M+1} = \sum_{\alpha=1}^{M} \boldsymbol{D}_{\alpha}\cdot\boldsymbol{P}(t)^{\mathrm{t}}\cdot\boldsymbol{F}_{\alpha} + \boldsymbol{D}\cdot P(t)^{\mathrm{t}}\cdot\boldsymbol{F}$$

The choice of the temporal finite elements of whom the shape functions depend on can be any *a priori*. In the present case, we will choose two-node elements.

The time integration of Eqs. (13a) and (13b) could be performed by a classical Gauss integration. In the present case, a nodal integration will be preferred. The integration points are thus the temporal nodes; with the ith node, corresponding to time t_i, will be associated the weight $\omega_i = \frac{1}{2}(\Delta t_i + \Delta t_{i+1})$, where $\Delta t_i = t_i - t_{i-1}$ and $\Delta t_{i+1} = t_{i+1} - t_i$ correspond to the lengths (or time steps) of the element that precedes and of the one that follows t_i (note the particular cases of the first and last nodes corresponding to the times t_1 and t_{N_T} for which the weights will be respectively equal to $\frac{1}{2}\Delta t_2$ and $\frac{1}{2}\Delta t_{N_T}$).

The advantage of the nodal time integration is that it decouples the components of the vector $\boldsymbol{\psi}_T$ in Eq. (13b), which are written now:

$$\forall i = 1,\ldots,N_t, \quad \psi_{i_T} = \omega_i\,\boldsymbol{D}^{\mathrm{t}}\cdot\boldsymbol{R}(t_i) = 0 \tag{14}$$

The resolution in time therefore consists in solving N_t non-linear scalar equations $\boldsymbol{D}^{\mathrm{t}}\cdot\boldsymbol{R}(t_i) = 0$.

4. Discussion on different strategies of resolution in elastoplasticity

The purpose of this paragraph is to describe the different strategies of calculation that have been considered for solving an elastoplastic problem.

The determination of $\boldsymbol{D}$ and $\boldsymbol{F}$ for each mode is based on the resolution of the coupled non-linear equations (13a) and (14). It is the exact resolution of these two systems of equations which will lead to an approximation made up of a minimal number of modes.

With this intention, Eq. (13a) could be solved by using a Newton–Raphson method to calculate $\boldsymbol{D}$ while supposing $\boldsymbol{F}$ (and thus $f(t)$) known. Then Eqs. (14) would be solved to calculate $\boldsymbol{F}$ while fixing $\boldsymbol{D}$ at the value previously found. Once the time function computed, one would go back to the resolution of Eq. (13a) and so on until convergence, as described in Algorithm 4.1. This method leads to solve an *a priori* large nonlinear system in space at each iteration of space–time coupling. This seems therefore expensive; in addition, the accurate resolution of the problem in space, whereas the time function is not yet well evaluated does not seem to be suitable.

Algorithm 4.1: First strategy of resolution.

Loop on PGD modes
  Space–Time coupling
    Space resolution
      Newton–Raphson method applied to Eq. (13a) for computing $\boldsymbol{D}$
    until convergence;
    Time resolution
      Newton–Raphson method to solve Eq. (14) for $i = 1,\ldots,N_t$
    until convergence;
  until convergence;
until PGD criterion *is reached*;

Unlike the first strategy, where two full resolutions in space and in time are successively carried out, another strategy for the resolution consists in considering the space–time problem as a whole and thus to link together until convergence a succession of calculations including an iteration of resolution of Eq. (13a) to correct $\boldsymbol{D}$ while supposing $\boldsymbol{F}$ known and followed by a resolution of Eq. (14) to calculate $\boldsymbol{F}$ while fixing $\boldsymbol{D}$ at the found value. The process is repeated until convergence, as it can be seen in Algorithm 4.2.

Algorithm 4.2: Second strategy of resolution.

Loop on PGD modes
  Resolution loop in Space and Time
    Newton–Raphson iteration for computing $\boldsymbol{D}$
    Newton–Raphson method to solve equation Eq. (14) for $i = 1, \ldots, N_t$
  until convergence;
until PGD criterion *is reached*;

A last strategy would be to no more strive to solve perfectly Eq. (13a). For each mode, $\boldsymbol{D}$ could thus be calculated assuming the behavior is elastic, *i.e.* by the resolution of a linear system derived from Eq. (13a), and be used then to solve Eq. (14) precisely. This leads to the method described in Algorithm 4.3. It is clear that this approach would lead to a number of modes larger than the one that would be obtained with one of the previous methods. But considering the resolution time, this method could appear as efficient.

Algorithm 4.3: Third strategy of resolution.

Loop on PGD modes
  Space linear resolution *for* $\boldsymbol{D}$
  Time resolution
    Newton–Raphson method to solve Eq. (14) for $i = 1, \ldots, N_t$
  until convergence *is reached*;
until PGD criterion *is reached*;

In all the cases, the convergence of the sequence will be supposed to be reached when:

$$\rho = \left(\frac{1}{\tau} \int_T \boldsymbol{R}(t)^{\mathrm{t}} \cdot \boldsymbol{R}(t) \, \mathrm{d}t \right)^{\frac{1}{2}} \leqslant \varepsilon_T \tag{15}$$

where $\boldsymbol{R}(t)$ is computed with the last solution obtained and ε_T is a desired accuracy threshold.

Remark 4.1 *(Resolution of Eqs. (14)).* The equations of the system of Eq. (14) being uncoupled, its resolution can be done step by step in time. Indeed, F_1 can be determined by the resolution of the first equation of Eq. (14). $\boldsymbol{D}^{\mathrm{t}} \cdot \boldsymbol{R}(t_1)$ being a function of F_1 only, the determination of F_1 can be done by a secant method. Then, knowing F_1, $\boldsymbol{D}^{\mathrm{t}} \cdot \boldsymbol{R}(t_2)$ becomes a function of F_2 only. The determination of F_2 can thus be done in the same way, and so on until $i = N_T$.

Full results such as the computing time and the convergence are not yet obtained. As it can be stated from Eqs. (13b) and (14), the PGD needs much more calculations of the instantaneous residuals $\boldsymbol{R}(t)$ than the step-by-step method, but, as a counterpart, far less resolutions of a global matrix system associated with the problem in space. It is thus expected that the efficiency of the method should be checked for large finite-element meshes in space and numerous time steps. The applications presented in the next section only contain few degrees of freedom; therefore their aim is only to validate the concepts of the method. A comprehensive study to compare the proposed strategies will be completed in a future work.

5. Applications

Modeling the ratcheting effect requires the implementation of complex models such as those described for example in [25] or [26].

In the present case, our goal is only to show the ability of the PGD to simulate the evolutions of the mechanical variables and therefore the ratcheting effect. This is why we have chosen to consider a von Mises elastoplastic material with nonlinear kinematic hardening of 'Armstrong–Frederick' type [27], known to lead to a constant ratcheting during cycles in the case of asymmetric cycles of imposed stresses. The law of evolution of the kinematic variable is given by:

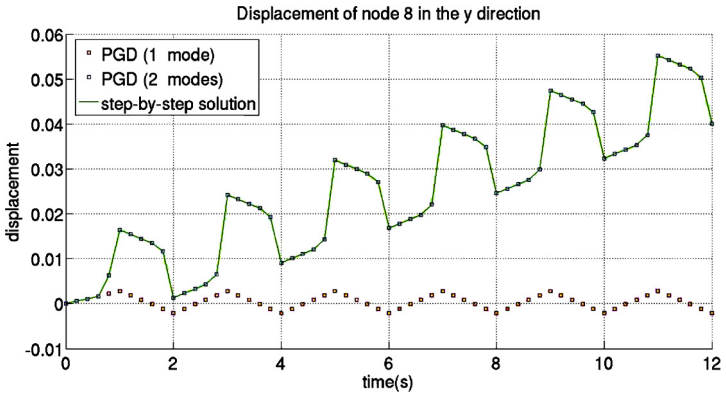

Fig. 1. Displacement of the end of the cube during cycles.

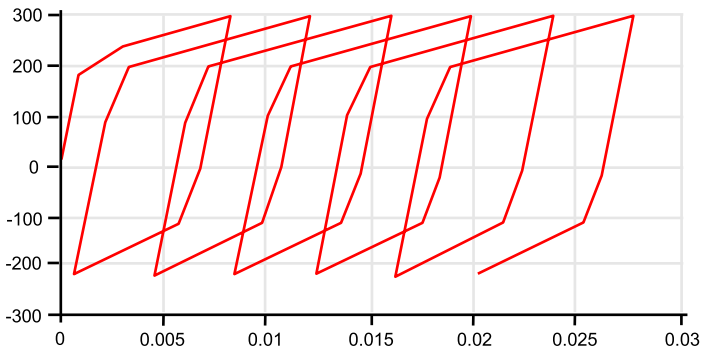

Fig. 2. Computed strain–stress cycles.

$$\dot{\chi} = \frac{2}{3} c\, \dot{\boldsymbol{\varepsilon}}^{\boldsymbol{p}} - \gamma\, \chi\, \dot{p} \tag{16}$$

where $\dot{\chi} = \frac{\mathrm{d}\chi}{\mathrm{dt}}$, $\boldsymbol{\varepsilon}^{\boldsymbol{p}}$ is the tensor of the plastic deformations, $\dot{p} = \sqrt{\frac{2}{3}\dot{\boldsymbol{\varepsilon}}^{\boldsymbol{p}} : \dot{\boldsymbol{\varepsilon}}^{\boldsymbol{p}}}$ is the cumulated equivalent plastic strain rate and c and γ are two parameters.

5.1. Uniaxial (tension–compression/traction and compression) test

The parameters of the model used in this case are for the Young modulus: $E = 210{,}000$ MPa, for the yield stress: $\sigma^y = 200$ MPa, $c = 25{,}000$ MPa, and $\gamma = 125$.

We consider a unit volume element subjected to uniaxial stress cycles between -220 MPa and 300 MPa.

Fig. 1 shows the displacement of the end of the cube during cycles with a step-by-step resolution and a PGD solution with two modes using Algorithm 4.3. In this example, the first mode has been calculated considering a fully elastic behavior. The second mode is therefore the first elastoplastic mode.

Fig. 2 gives the evolution of the axial stress as a function of the axial deformation. These two figures clearly highlight the ratcheting effect and the ability of the PGD to reproduce it. It should be noted that the time steps used for the PGD being the same as those used for the step-by-step resolution, the error made for the integration of the constitutive equations is the same in both cases.

5.2. Perforated plate subjected to a monotonic loading

We now consider a perforated plate whose mesh and loading are given in Fig. 3. The behavior model used here is an isotropic work hardening one (Young modulus: $E = 210{,}000$ MPa, Poisson coefficient $\nu = 0,3$, yield stress $\sigma^y = 100$ MPa, hardening slope 5000 MPa). A monotonic pressure is applied from 0 to 75 MPa. Figs. 4 and 5 give the axial displacement of node 35 and the transverse displacement of node 53 over time and show the ability of the PGD to give a quite satisfying solution from only 2 modes using algorithm 3. Here again, the first mode is a fully elastic mode.

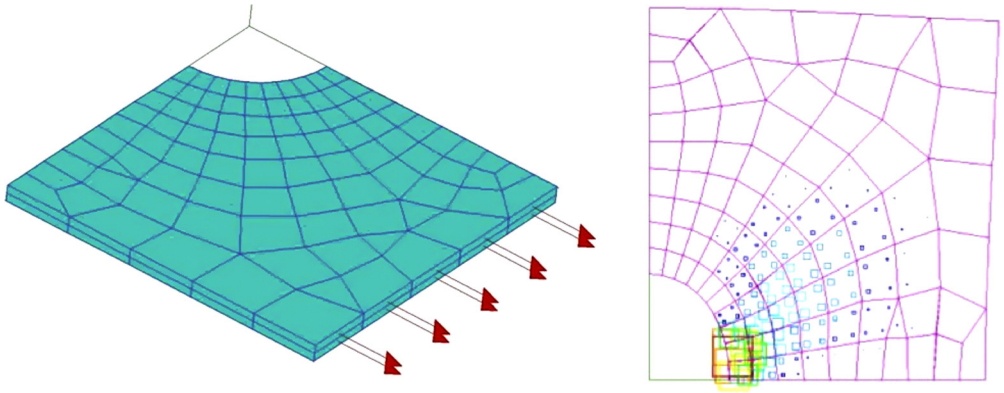

Fig. 3. Mesh and loading of the perforated plate – Plastic zone at 75 MPa.

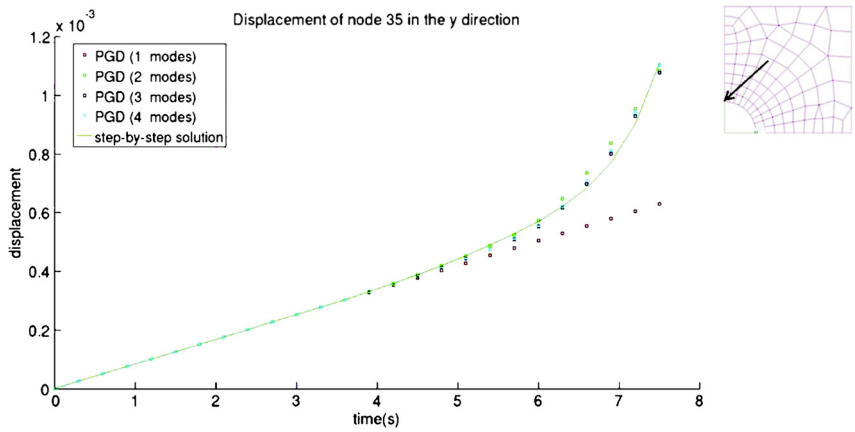

Fig. 4. Axial displacement of node 35 over time.

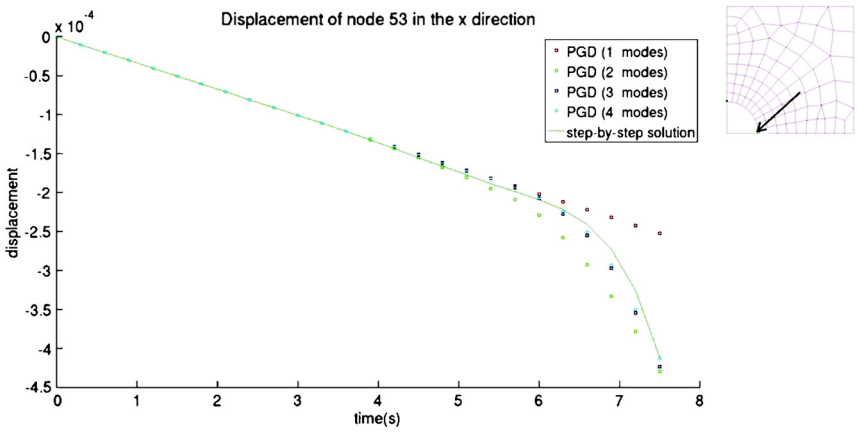

Fig. 5. Transverse displacement of node 53 over time.

5.3. *Perforated plate subjected to a cyclic loading*

We take again the nonlinear kinematic hardening model used previously for the cube and the cyclic loading described in Fig. 6 is applied to the plate. The parameters of the model used in this case are $E = 210{,}000$ MPa, $\nu = 0,3$, $\sigma^y = 100$ MPa, $c = 25{,}000$ MPa, and $\gamma = 125$.

Figs. 7 and 8 giving the axial displacement of node 35 and the transverse displacement of node 53 show the convergence of the method, using Algorithm 4.2. The loading being far more complex than the monotonic loading considered previously,

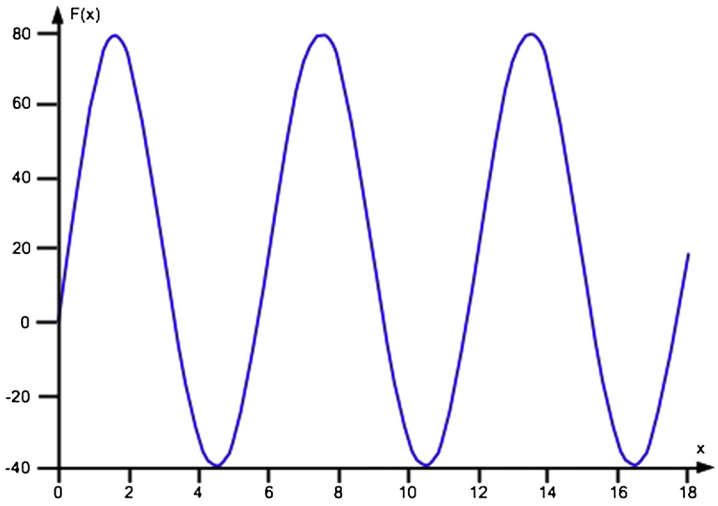

Fig. 6. Cyclic loading of the perforated plate.

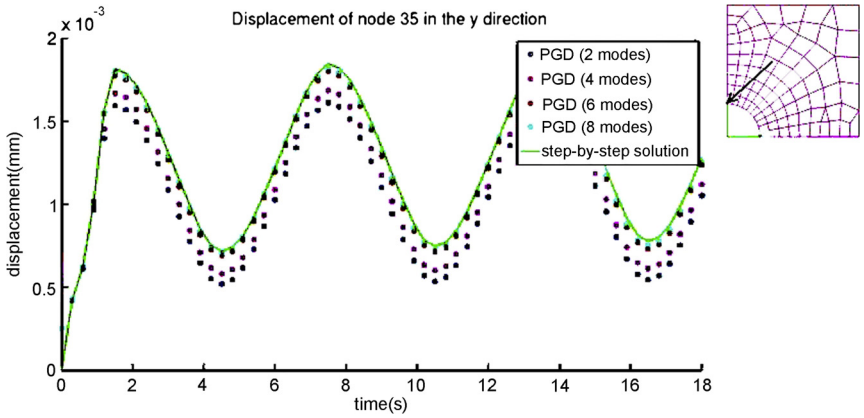

Fig. 7. Axial displacement of node 35 over time.

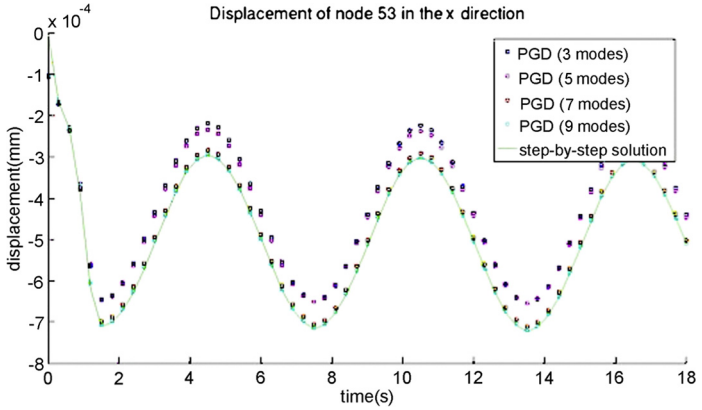

Fig. 8. Transverse displacement of node 53 over time.

an accurate solution with the PGD requires more modes. Fig. 9 is giving the axial stress evolution as a function of the axial deformation in the element located near the hole reveals, during first cycles, a phenomenon of progressive deformation combined with an average stress relaxation.

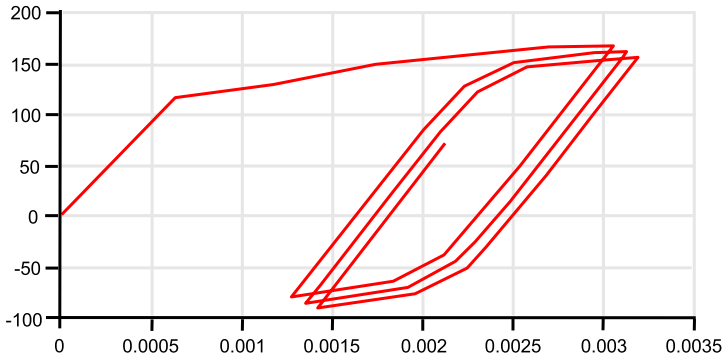

Fig. 9. Evolutions of the axial stress as a function of the axial deformation.

6. Conclusion

The PGD was successfully applied for simulating elastoplastic problems with the choice of a finite element method for the approximation both in space and in time. The method leads to solve two coupled nonlinear problems, one in space and one in time, and the same approach can be applied to other constitutive equations.

The first results are promising. They show the ability of the PGD to simulate complex cyclic evolutions with ratcheting effects. The more complex is the evolution of the loading of course in space but also in time, the bigger is the number of modes necessary to obtain a satisfying solution.

As it has been explained in section 4, different strategies can be used to solve the coupled space–time problem. Full results relative to the computing time and the convergence will be completed in a future work.

References

[1] J. Zarka, J. Frelat, G. Inglebert, P. Kasmai-Navidi, A New Approach in Inelastic Analysis of Structures, CADLM, Gif-sur-Yvette, France, 1990.
[2] A. Benoit, M.-H. Maitournam, L. Rémy, F. Oger, Cyclic behaviour of structures under thermomechanical loadings: application to exhaust manifolds, Int. J. Fatigue 38 (2012) 65–74.
[3] K.V. Spiliopoulos, K.D. Panagiotou, A direct method to predict cyclic steady states of elastoplastic structures, Comput. Methods Appl. Mech. Eng. 223 (224) (2012) 186–198.
[4] M. Peigney, C. Stolz, An optimal control approach to the analysis of inelastic structures under cyclic loading, J. Mech. Phys. Solids 51 (4) (2003) 575–605.
[5] M.-H. Maitournam, B. Pommier, J.-J. Thomas, Determination of the asymptotic response of a structure under cyclic thermomechanical loading, C. R. Mecanique 330 (10) (2002) 703–708.
[6] P.-M. Lesne, S. Savalle, An efficient cycle jump technique for viscoplastic structure calculations involving large number of cycles, in: 2nd Int. Conf. on Computational Plasticity, Barcelona, Spain, 1989, pp. 591–602.
[7] J.-L. Chaboche, G. Cailletaud, Integration methods for complex plastic constitutive equations, Comput. Methods Appl. Mech. Eng. 133 (1996) 125–155.
[8] P. Boisse, P. Bussy, P. Ladevèze, A new approach in non-linear mechanics: the large time increment method, Int. J. Numer. Methods Eng. 29 (1990) 647–663.
[9] J.-Y. Cognard, P. Ladevèze, A large time increment approach for cyclic viscoplasticity, Int. J. Plast. 9 (1993) 141–157.
[10] F. Comte, M.-H. Maitournam, P. Burry, T. Mac Lan Nguyen, A direct method for the solution of evolution problems, C. R. Mecanique 334 (2006) 317–322.
[11] A. Ammar, M. Normandin, F. Chinesta, Solving parametric complex fluids models in rheometric flows, J. Non-Newton. Fluid Mech. 165 (2010) 1588–1601.
[12] E. Pruliere, F. Chinesta, A. Ammar, On the deterministic solution of multidimensional parametric models by using the Proper Generalized Decomposition, Math. Comput. Simul. 81 (2010) 791–810.
[13] F. Chinesta, R. Keunings, A. Leygue, The Proper Generalized Decomposition for Advanced Numerical Simulations: A Primer, SpringerBriefs Appl. Sci. Technol., Springer, 2014.
[14] J.L. Lumley, The structure of inhomogeneous turbulent flows, in: A.M. Yaglom, V.I. Tatarsky (Eds.), Atmospheric Turbulence and Radio Wave Propagation, Moscow, 1967, pp. 166–178.
[15] C. Germoso, J.V. Aguado, A. Fraile, E. Alarcon, F. Chinesta, Efficient PGD-based dynamic calculation of non-linear soil behavior, C. R. Mecanique 344 (1) (2016) 24–41.
[16] M. Hammoud, M. Beringhier, J.-C. Grandidier, A reduced simulation applied to the viscoelastic fatigue of polymers, C. R. Mecanique 342 (2014) 671–691.
[17] A. Ammar, A. Zghal, F. Morel, F. Chinesta, On the space–time separated representation of integral linear viscoelastic models, C. R. Mecanique 343 (4) (2015) 247–263.
[18] R. De Borst, M.A. Crisfield, J.J. Remmers, C.V. Verhoosel, Nonlinear Finite Element Analysis of Solids and Structures, John Wiley & Sons, 2012.
[19] P. Wriggers, Nonlinear Finite Element Methods, Springer Science & Business, Media, 2008.
[20] Q. Nguyen, On the elastic plastic initial-boundary value problem and its numerical integration, Int. J. Numer. Methods Eng. 11 (1977) 817–832.
[21] J. Simo, T. Hughes, Computational Inelasticity, Springer-Verlag, New York, 1998.
[22] K.J. Bathe, Finite Element Procedures, Prentice–Hall, 1996.
[23] W. Hu, P.F. Thomson, An evaluation of a large time increment method, Comput. Struct. 58 (1996) 633–637.
[24] P. Despret, Simulation numerique de la solidification avec reduction de modele PGD appliquée à la fonderie, PhD thesis, University of Technology of Compiègne, France, 2015 (in French).
[25] H. Burlet, C. Cailletaud, Modeling of cyclic plasticity in finite element codes, in: C.S. Desai (Ed.), 2nd Int. Conf. on Constitutive Laws for Engineering Materials: Theory and Applications, Elsevier, Tucson, AZ, USA, 1987, pp. 1157–1164.
[26] J.-L. Chaboche, A review of some plasticity and viscoplasticity constitutive theories, Int. J. Plast. 24 (2008) 1642–1693.
[27] P.J. Armstrong, C.O. Frederick, A mathematical representation of the multiaxial Bauschinger effect, CEGB report No. RD/B/N 731, UK, 1966.